

Antiferromagnetic coupling between martensitic twin variants observed by magnetic resonance in Ni-Mn-Sn-Co films

V. O. Golub,¹ V. A. Lvov,^{1,2} I. Aseguinolaza,³ O. Salyuk,¹ D. Popadiuk,⁴ Y. Kharlan,⁴ G. N. Kakazei,⁵ J. P. Araujo,⁵ J. M. Barandiaran,³ and V. A. Chernenko^{3,6,*}

¹*Institute of Magnetism of the National Academy of Sciences and Ministry of Education and Science of Ukraine, Kyiv 03142, Ukraine*

²*Taras Shevchenko National University of Kyiv, Kyiv 01601, Ukraine*

³*BCMaterials & University of Basque Country, P.O. Box 644, Bilbao 48080, Spain*

⁴*National Technical University of Ukraine "KPI," Kyiv 03056, Ukraine*

⁵*Instituto de Física dos Materiais da Universidade do Porto - Instituto de Nanociência e Nanotecnologia, Departamento de Física e Astronomia, Universidade do Porto, 4169-007 Porto, Portugal*

⁶*Ikerbasque, Basque Foundation for Science, Bilbao 48013, Spain*

(Received 10 August 2016; revised manuscript received 27 December 2016; published 23 January 2017)

Magnetic properties of Ni_{46.0}Mn_{36.8}Sn_{11.4}Co_{5.8}/MgO(001) epitaxial thin film, which undergo a martensitic phase transformation from cubic austenitic phase to a twinned orthorhombic martensitic phase at 270 K, were studied by the magnetic resonance at the microwave frequency of 9.45 GHz. It was found that the single resonance line observed in the austenite splits into three lines in the martensitic phase. A theoretical approach was developed to show that the additional resonance lines are caused by the weak antiferromagnetic coupling of the ferromagnetic twin components across twin boundaries. Fitting of the experimental resonance lines to model gives an effective field of antiferromagnetic coupling of about 1.5 kOe, which is two or three orders of magnitude lower than in the conventional antiferromagnetic solids because the number of magnetic ions interacting antiferromagnetically through the twin boundary is much less than the total number of magnetic ions in the twin. This feature shows a strong resemblance between the submicron twinned martensite and artificial antiferromagnetic superlattices, whereby providing a distinctive insight into magnetism of the studied magnetic shape memory material.

DOI: [10.1103/PhysRevB.95.024422](https://doi.org/10.1103/PhysRevB.95.024422)

I. INTRODUCTION

Heusler-type magnetic shape memory alloys (MSMAs) are of great interest due to both their unusual physical properties and potential applications in different areas of science and technology [1]. Historically, the interest arose from the magnetic shape memory effect, also called the magnetic field induced strain, which results in a dramatic change of the sample dimensions (up to 12%) in moderate magnetic fields due to twin boundary motion in the martensitic state [2–4]. Later investigations revealed many other effects in these materials, which are also related to the martensitic transformation (MT). Among these effects are the magnetic superelasticity, direct and inverse magnetocaloric effect, giant magnetoresistance, exchange bias, etc. [4–6]. Some MSMAs are half metallic and can provide a hundred percent spin polarized electrons, a very attractive feature for spintronics applications [7,8].

From a basic point of view, MSMAs are interesting because they can exhibit sequences of structural transformations (premartensitic, martensitic, and intermartensitic), as well as magnetic phase transitions. In some alloys the temperature of the first order martensitic transformation coincides with the temperature of ferromagnetic ordering, so the first order magnetostructural phase transition takes place [6,9]. In these alloys, the external magnetic field can control MT. Such first order magnetostructural phase transitions are also accompanied by large magnetization changes, as well as giant magnetoresistance, magnetocaloric, and Hall effects [6,9,10].

Ni-Mn-Ga Heusler alloys are among the most studied MSMAs. The MT in these alloys takes place from a ferromagnetic austenite to a ferromagnetic martensite with only a small increase of the saturation magnetization of martensite in comparison with that of austenite. These alloys are called ferromagnetic shape memory alloys.

In contrast to Ni-Mn-Ga alloys, the Ni₅₀Mn_{50–y}Z_y (Z = In, Sn, Sb) alloys show unusual magnetostructural phase transition from the ferromagnetic austenite to a weakly magnetic or nonmagnetic martensite (see Refs. [4,6,9] and references therein). Typically, they are doped by Co or Fe atoms instead of Ni to tune mutual position of the Curie temperature of austenite and the MT temperature as well as enhance a magnetization jump at MT. All these alloys are referred to as meta-MSMAs (MMSMAs). They exhibit a giant inverse magnetocaloric effect at the transition, which makes them promising for magnetic refrigeration [4–6,11,12].

In the early articles, the magnetostructural transition in MMSMAs was interpreted as a transition from ferromagnetic austenite to paramagnetic martensite (see Ref. [13] and references therein). But further investigations have shown a much more complex situation, as the magnetic susceptibility of the nonmagnetic martensite was too high to be attributed to the usual paramagnetic behavior; consequently, it was ascribed to the formation of the superparamagnetic clusters in the paramagnetic matrix [14–16]. However, this explanation does not have a universal character for all Ni₅₀Mn_{50–y}Z_y-based MMSMAs. The magnetostructural phase transitions in such materials were theoretically studied by first principles calculations (see, e.g., Refs. [17,18] and references therein). According to these calculations, there exists an interplay of antiferromagnetic and ferromagnetic exchange interactions

*volodymyr.chernenko@ehu.es

between the magnetic ions, which leads to dramatic changes of the magnetic properties in the magnetostructural phase transition. In particular, the MT leads to the suppression of ferromagnetism manifested in a drastic decrease of saturation magnetization.

Neutron scattering and ferromagnetic resonance experiments carried out on powders of these materials showed the presence of some local antiferromagnetic coupling between the particles of powder [19]. This was also supported by the low temperature field-cooled magnetization loops measurements, which showed the characteristic shift due to the exchange bias. However, the nature of the antiferromagnetic coupling in $\text{Ni}_{50}\text{Mn}_{50-y}\text{Z}_y$ alloys is not explained well yet. Moreover, the character of the magnetic ordering in the martensitic phase is seemingly neither the same in these materials nor even known for many of them [20].

Herewith, we report the study of magnetic properties of $\text{Ni}_{46.0}\text{Mn}_{36.8}\text{Sn}_{11.4}\text{Co}_{5.8}$ epitaxial film by ferromagnetic resonance to shed light on the magnetic ordering of the twinned martensitic phase formed as a result of magnetostructural transition in this kind of MMSMA. Previously, in Ni-Mn-Ga ferromagnetic thin films, we found the strong exchange coupling of ferromagnetic type between submicron twin components, which resulted in an averaged magnetic anisotropy. Due to the ferromagnetic exchange coupling between the twin components, their magnetic moments became parallel to each other, and the magnetic domains spreading through the large number of neighboring twins were formed [21,22]. Contrary to these findings, our present study of martensitic MMSMA film indicates the presence of weak antiferromagnetic coupling between the ferromagnetically ordered twin components. This coupling can explain the exchange bias and magnetic resonance spectra, as also the case in antiferromagnetically coupled multilayered structures [23]. The resemblance between the artificial antiferromagnetic superlattices (see, e.g., Ref. [24]) and twinned martensitic films of MMSMA provides an argument for the importance of study of these films. The observed self-assembled effect is similar to nano-patterning and therefore can be considered as relevant for the magnonic applications (to achieve tunable resonance fields/frequencies) [25].

II. EXPERIMENTAL

A 1 μm -thick $\text{Ni}_{46.0}\text{Mn}_{36.8}\text{Sn}_{11.4}\text{Co}_{5.8}$ film was deposited by DC magnetron sputtering onto a heated (500 $^{\circ}\text{C}$) single crystalline MgO (001) substrate, using an Argon pressure of $1.1 \cdot 10^{-2}$ mbar and a power of 150 W. The composition of the film was determined by energy-dispersive x-ray (EDX) spectroscopy with an accuracy better than 0.5 at.%. The x-ray structural analysis confirmed an epitaxial growth of the film with one of its crystallographic cubic (100) axes oriented along out-of-plane $[001]_{\text{MgO}}$ direction and two others oriented along in-plane $\langle 110 \rangle_{\text{MgO}}$ directions, in agreement with the usually observed epitaxial MSMA structures grown on MgO [26–29]. The x-ray diffraction also revealed an orthorhombic unit cell of the martensitic phase. In contrast with Ref. [22], direct scanning electron microscopy (SEM) observation of the twin structure was not possible because of the surface roughness of the present films.

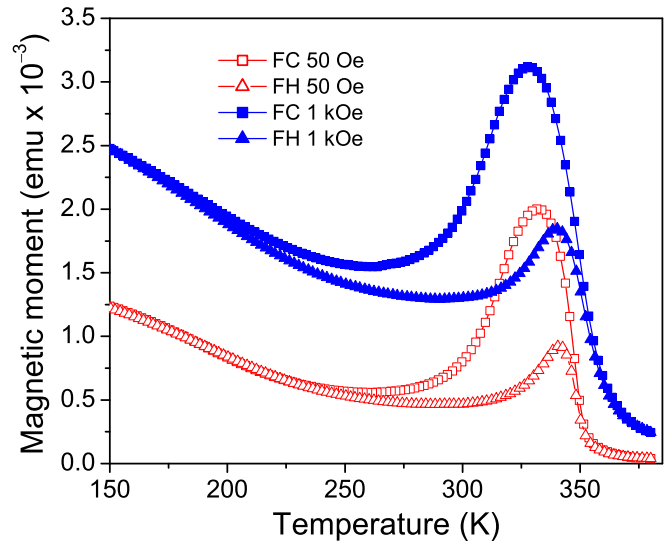


FIG. 1. Temperature dependences of magnetization of the $\text{Ni}_{46.0}\text{Mn}_{36.8}\text{Sn}_{11.4}\text{Co}_{5.8}/\text{MgO}(001)$ film measured during the field-cooling (FC) and field-heating (FH) ramps in the fields of 50 Oe and 1 kOe. The magnetic field is applied in the film plane.

Magnetic characterization of the film was performed in the temperature range of 5–400 K using a Quantum Design MPMS 5S SQUID magnetometer. Magnetic resonance measurements were carried out in the temperature range of 100–450 K by the electron spin resonance spectrometer Bruker ELEXSYS E500 operating at 9.46 GHz (X-band) equipped with the automatic goniometer.

The field-cooling (FC) and field-heating (FH) magnetization curves are presented in Fig. 1. Cooling down of the sample

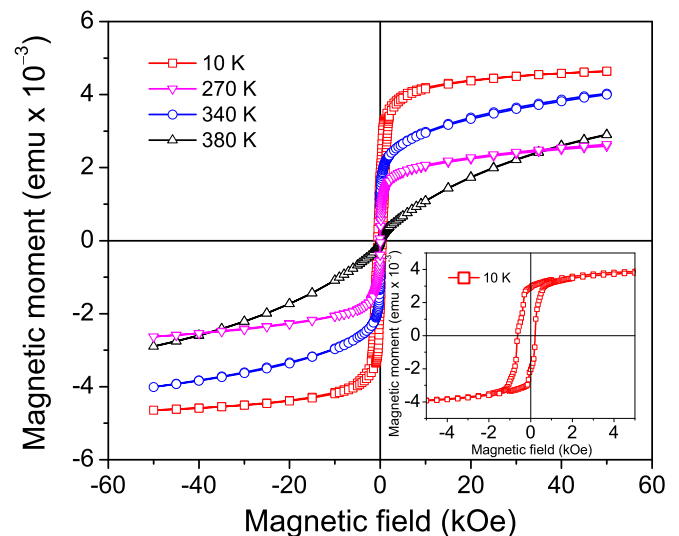


FIG. 2. The magnetization loops of the $\text{Ni}_{46.0}\text{Mn}_{36.8}\text{Sn}_{11.4}\text{Co}_{5.8}/\text{MgO}(001)$ film measured at different temperatures. The temperatures 10 K and 270 K correspond to the martensitic state of the sample. At 340 K, the sample is in ferromagnetic austenitic state. The temperature of 380 K is around the Curie temperature. The hysteresis loop recorded at 10 K for the sample cooled down in the magnetic field of 50 kOe is shown in the inset.

below 370 K (Curie point) results in the rapid increase of magnetization value due to the phase transition from paramagnetic to ferromagnetic austenite. Further cooling across MT leads to the decrease of magnetization of the sample. This decrease is attributed to the increase of magnetic anisotropy in martensitic phase and the decrease of the saturation magnetization, as also evident from Fig. 2. Further cooling results in a gradual increase of magnetization. The magnetization measured in the field of 1 kOe at 150 K is comparable in value with magnetization of austenitic phase. It points to ferromagnetic ordering of martensitic phase. Temperature hysteresis of the magnetization curves is related to the first order character of MT.

It is worth noting that the hysteresis loop recorded in the martensitic state is shifted along the x axis for the sample cooled down in the magnetic field (see inset in Fig. 2). Such a behavior (exchange bias) is usually associated with the presence of the antiferromagnetic coupling at boundaries of different layers (see, e.g., Ref. [10]). In our case, coercive and bias field values at 10 K are $H_C = 380$ Oe and $H_B = 180$ Oe, respectively.

Figure 3(a) shows temperature evolution of the resonance spectra measured during step-wise heating in the external magnetic field directed perpendicular to the film plane. The intensity of the spectra is the linear function of the radiofrequency power. Three inhomogeneously broadened lines (corresponding to the resonance fields H_{R1} , H_{R2} , and H_{R3}) have been observed in the martensitic state, below the room temperature [see Figs. 3(a) and 3(b)]. Above room temperature (in the temperature range of martensite-austenite transformation), a new line (H_R) appears [Figs. 3(a) and 3(c)]. Figure 4 shows the temperature dependences of the resonance fields extracted from the spectra. As seen in the figure, the lines H_{R1} , H_{R2} , and H_{R3} are observed in the temperature range of $100 \text{ K} < T < 260 \text{ K}$, whereas in the temperature interval of $260 \text{ K} < T \leq 360 \text{ K}$ the lines H_R , H_{R1} , and H_{R2} are present. At higher temperatures, $T > 360 \text{ K}$, only one line (H_R), which is typical for the austenitic Heusler MSMA [21], is observed.

It is worth noting that the intensity of line H_R increases on heating, reaching maximum value at 380 K. In the same time, the intensities of the lines observed in the martensitic state gradually decrease and disappear. Further heating leads to the decrease of the resonance field value H_R (see Fig. 4) accompanied by the reduction of its intensity to the values, which are typical for paramagnetic materials. It is quite typical for Heusler MSMA, exhibiting MT, that an inhomogeneously broadened line is observed in the martensitic phase, while a rather narrow resonance line [with antisymmetric derivative shown in Fig. 3(c)], whose amplitude and resonance field rapidly decrease near the Curie temperature, is detected in the austenitic phase (see, e.g., Ref. [21]).

The occurrence of three resonance lines in the martensitic state of studied film demonstrates a striking difference between the magnetic state of this film and Ni-Mn-Ga martensitic film showing one resonance only [22]. In the latter case, the overall resonance behavior was brought about by a strong ferromagnetic exchange coupling across twin boundaries [22]. To understand a puzzling behavior in the former case, in the next sections, the additional experimental data are shown, and the original theoretical approach is developed.

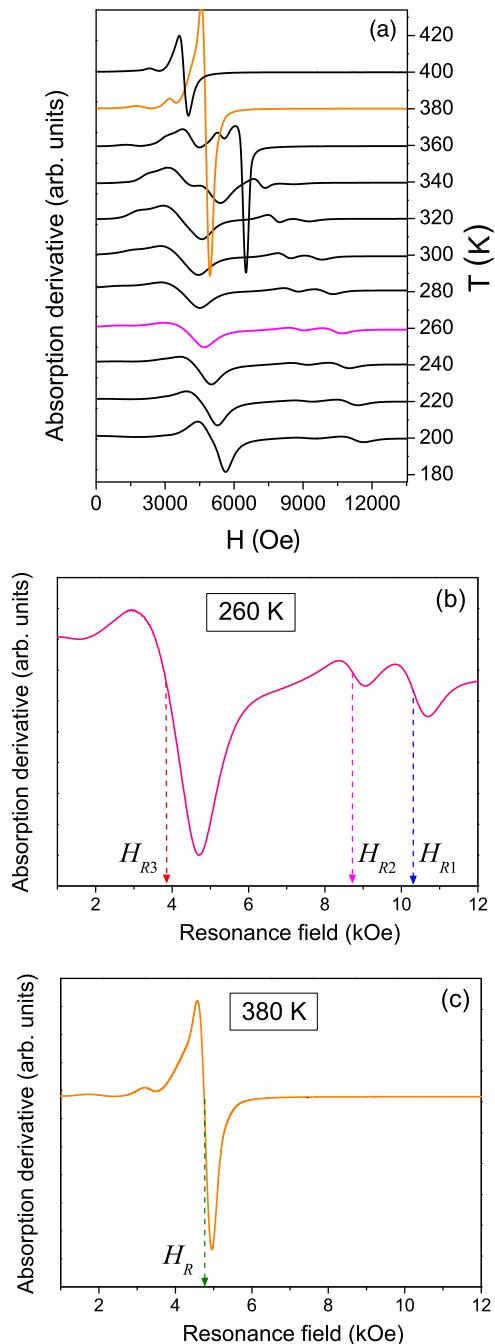


FIG. 3. Resonance spectra recorded at different temperatures for $\text{Ni}_{46.0}\text{Mn}_{36.8}\text{Sn}_{11.4}\text{Co}_{5.8}/\text{MgO}(001)$ film under magnetic field applied perpendicular to the film plane (a); rescaled images of the representative spectra (b) and (c). Paramagnetic admixture lines from the film and the substrate (not analyzed in this paper) are observed in the range of 3000–4000 Oe. The vertical arrows in (b) and (c) point to the resonance field values H_{R1} , H_{R2} , and H_{R3} , explained in Sec. IV.

III. ADDITIONAL MEASUREMENTS AND QUALITATIVE ANALYSIS OF THE DATA

The appearance of three lines in one ferromagnetic phase of the film cannot be explained in terms of spin wave resonance in the ferromagnetic film. At first sight, the observation of three resonance lines in the martensitic film suggests the formation

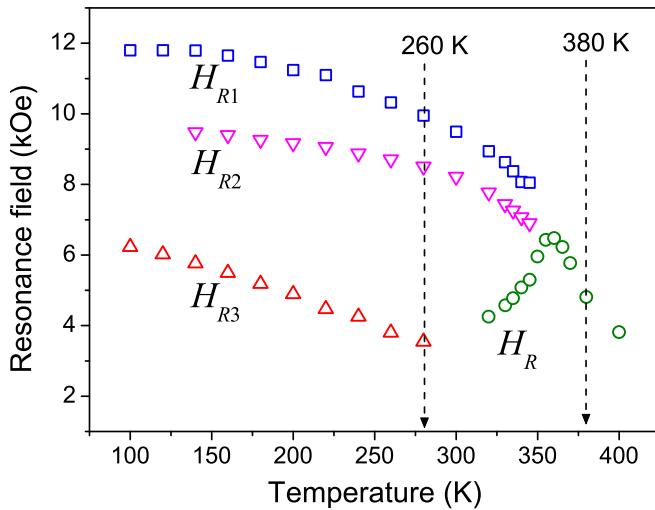


FIG. 4. Temperature dependences of the resonance fields measured for $\text{Ni}_{46.0}\text{Mn}_{36.8}\text{Sn}_{11.4}\text{Co}_{5.8}/\text{MgO}(001)$ film. The external magnetic field is perpendicular to the film plane. Triangles and squares depict the positions of three peaks detected in martensite (see in the text), and circles show the position of peak in austenite. Vertical arrows point to the temperatures corresponding to the resonance peaks shown in Figs. 3(b) and 3(c).

of few different magnetic phases below the MT temperature. For instance, three ferromagnetic phases might be expected: Two of them have higher saturation magnetization and Curie temperature, which are close to the Curie temperature of austenite, while the third one has relatively low magnetization and Curie temperature around 270 K. However, magnetic measurements did not indicate the formation of different magnetic phases near 270 K: No peculiarities, which could be attributed to the formation of these phases, are detected on the temperature dependence of magnetization (see Fig. 1). The possible formation of defect regions near the substrate surface below the MT point is also not able to explain the resonance spectra splitting observed experimentally. In the case of defect area formation, it is unlikely to expect a formation of the large enough homogeneous magnetic regions with the same magnetic parameters. Much more probable would be the inhomogeneous distribution of magnetically ordered areas, which will lead to inhomogeneous line broadening rather than resonance spectrum splitting into several quite symmetrical lines. The existence of some antiferromagnetically ordered areas in the film can be inferred from the observed shift of the hysteresis loop (exchange bias) at low temperatures (see inset in Fig. 2). Thus, the observed resonance spectrum can be explained only by a formation of homogeneous antiferromagnetic areas with the same magnetic parameters. The defect area formation mechanism can provide a path for antiferromagnetic phase appearance in this compound (see below) and can explain the observed exchange bias at low temperature, but, again, these areas should have different magnetic parameters (Neel temperature, magnetic anisotropy, etc.), which would lead to inhomogeneous lines broadening instead of the spectrum splitting.

Note that the observed magnetic resonance spectrum is impossible to explain in terms of domain walls resonance

because at least two of three peaks were observed at saturated magnetic fields, i.e., when there are no magnetic domains and domain walls. Incidentally, the domain walls resonance (not presented here) was observed for this film in the low magnetic field area, well below discussed resonance line position, and appeared to be dependent on the magnetic field sweep direction.

The observation of two peaks in a saturated state allows excluding magnetostatic interaction between twin variants as well. The magnetostatic interaction between twin variants should result in the observation of two resonance peaks in saturating fields both for antiferromagnetic interaction between twin components and also for the ferromagnetic coupling of these components. However, previously [21,22,25] only one resonance peak was observed in quite similar twinned films of ferromagnetic Ni-Mn-Ga alloys but with ferromagnetic coupling between twin components. This experimental fact allows for the disregarding of the magnetostatic coupling for other fine-twinning ferromagnetic films.

In the case of one antiferromagnetic phase formed below the MT temperature, only two resonance peaks should be observed [30]. It is well known, moreover, that in the classical antiferromagnets, these peaks correspond to the two resonance modes, optical and acoustical. The interval between acoustical and optical branches of the resonance spectrum is about of hundreds or thousands gigahertz [30]. As so, the optical mode cannot be observed at our experimental conditions in the case of classical antiferromagnetic phase. Observation of acoustic and optical modes could be possible at such conditions in the experiments with synthetic antiferromagnets, i.e., multilayered structures of ferromagnetic films coupled by the *weak* antiferromagnetic exchange (usually through nonmagnetic interlayers) [31]. In such antiferromagnets, the distance between optical and acoustic mode can be reduced to several gigahertz (several kilooersted). In our case, the formation of structure that is similar to the synthetic antiferromagnet is possible due to the submicron twinning of martensite: The ferromagnetically ordered twin components may be antiferromagnetically coupled by the reasons explained below.

As mentioned in Sec. II, the single-crystalline $\text{MgO}(001)$ substrate provides an epitaxial growth of $\text{Ni}_{46.0}\text{Mn}_{36.8}\text{Sn}_{11.4}\text{Co}_{5.8}$ film in the austenitic state. The condition of the surface area conservation prescribes the transition of the film into the martensitic state through fine twinning [22,27–29]. In the $\text{Ni}_{50}\text{Mn}_{50-y}\text{Z}_y$ ($Z = \text{In, Sn, Sb}$) alloys, the type of exchange coupling between the magnetic ions depends on their spatial arrangement and distances between them. Due to this, it is possible to get a situation when the exchange is ferromagnetic inside the twins and antiferromagnetic at the twin boundaries. It is also important that the twin boundary is a practically ideal plane. This feature provides a uniform exchange across the twin boundary. Twins width in the epitaxial films of Heusler alloys is about of several tens of nanometers [22,27–29], thus comparable with the exchange correlation length [22]. So the twin components can be antiferromagnetically coupled due to the exchange interaction. The proof of such coupling can be deduced from the characteristic dependence of the in-plane resonance fields on the angle between the external field and [100] crystallographic direction in MgO substrate. In this regard, we additionally have measured angle dependences of

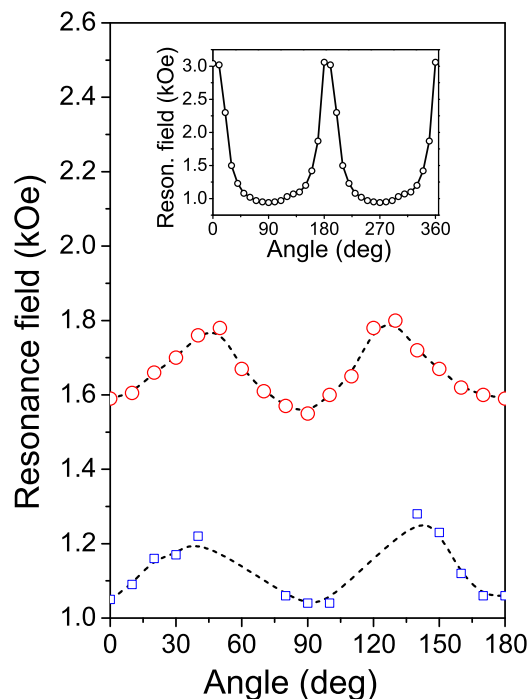


FIG. 5. The experimental angular dependence of the resonance fields in the film plane for two resonance peaks observed at 273 K (symbols). The dashed lines are guides for the eye. The angular dependence of the resonance field measured for the martensitic Ni-Mn-Ga film, which does not exhibit an exchange coupling, is shown in the inset for comparison (see Ref. [26]).

resonance fields, which are depicted in Fig. 5. A 90° periodicity of the resonance field is found in the martensitic state (Fig. 5). This periodicity is inherent in the epitaxially grown submicron twinned MSMA films [22]. In contrast to this, a 180° periodicity of the resonance field is typical to the non-epitaxial MSMA films exhibiting orthorhombic martensite and lacking exchange coupling between twin components [26] (see inset in Fig. 5). The idea about the antiferromagnetic coupling between twin components has achieved a quantitative confirmation within the theoretical approach developed in the next section.

IV. THEORY

According to the idea about the weak antiferromagnetic coupling of twin components, let us consider the twin components with magnetization vectors \mathbf{M}_1 and \mathbf{M}_2 interacting with each other through the magnetic exchange of the antiferromagnetic type. The theory of antiferromagnetic resonance (AFMR) in the antiferromagnets with two magnetic sublattices is commonly known [30]. This theory can be adapted to the case of two twin components. For this purpose, it is convenient to express the free energy density of twin as the sum of free energies F_1 and F_2 of twin components and the energy F_{12} of spin exchange interaction between the twin components:

$$\begin{aligned}
 F &= F_1 + F_2 + F_{12}, \\
 F_1 &= \frac{1}{2}\beta M_{1z}^2 - \mathbf{M}_1 \mathbf{H}, \\
 F_2 &= \frac{1}{2}\beta M_{2z}^2 - \mathbf{M}_2 \mathbf{H}, \\
 F_{12} &= \delta \mathbf{M}_1 \mathbf{M}_2,
 \end{aligned} \tag{1}$$

where the dimensionless parameters β and δ are referred to as the anisotropy constant and exchange constant, respectively; \mathbf{H} is the magnetic field; and the first and second terms in the right sides of equations for F_1 and F_2 are the magnetic anisotropy energy densities and Zeeman energy densities in twin components, respectively. The twin components are considered physically equivalent, therefore, $|\mathbf{M}_1| = |\mathbf{M}_2| \equiv M(T)$. It is shown below that the temperature dependence of magnetization of martensitic film is satisfactorily described by the standard equation

$$M(T) = M(0) \tanh [T_C M(T) / T M(0)] \tag{2}$$

It is convenient to characterize the film by the temperature dependent anisotropy field $H_A(T) = \beta M(T)$ and exchange field $H_E(T) = \delta M(T)$.

The antiparallel orientation of magnetization vectors diminishes the free energy of twin if $\delta > 0$. According to experimental data shown in Fig. 5 and theoretical considerations presented in Ref. [22], the internal twinning reduces the uniaxial magnetocrystalline anisotropy of the film almost to zero. In this case $\beta \approx 4\pi > 0$; therefore, the magnetostatic field of the film orients the magnetization vectors in the film plane (see Fig. 6). As shown in Fig. 6, the magnetic field $H_z \equiv H$, applied normal to the film, turns the magnetization vectors in fixed plane, which can be considered as the yz plane of coordinate system. In this case, equilibrium values, \overline{M}_{1i} and \overline{M}_{2i} , of magnetization vector components, M_{1i} and M_{2i} , satisfy the relationships

$$\begin{aligned}
 \overline{M}_{1x} &= \overline{M}_{2x} = 0, \\
 \overline{M}_{1y} &= -\overline{M}_{2y} = M(T) \sin \theta(H, T), \\
 \overline{M}_{1z} &= \overline{M}_{2z} = M(T) \cos \theta(H, T),
 \end{aligned} \tag{3}$$

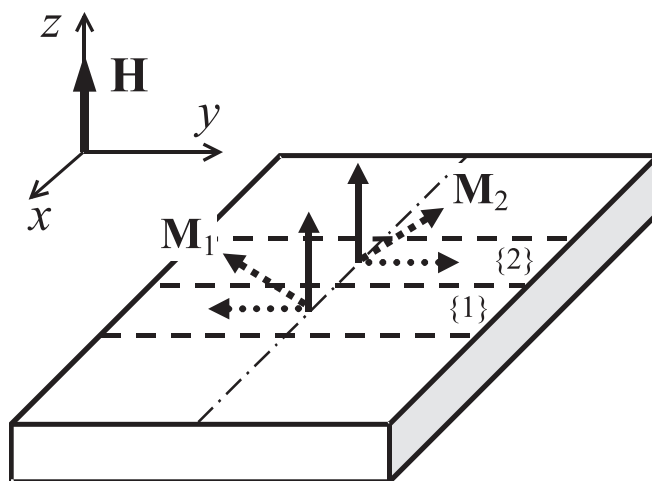


FIG. 6. Schematic of the twinned magnetic film in the perpendicular external magnetic field. Twin boundaries are shown by the dashed lines. The numbers {1} and {2} mark the twin components. The dotted, dashed, and solid arrows show the directions of the magnetization vectors for the field values $H = 0$, $H < H_{A-F}$, and $H > H_{A-F}$, respectively. Here, H_{A-F} is the field of phase transition of twins from antiferromagnetic to ferromagnetic state.

where $\theta(H, T)$ is the angle between the vectors \mathbf{M}_1 and \mathbf{H} . The minimum conditions for the free energies [Eq. (1)] result in the equation

$$\cos \theta(H, T) = \begin{cases} H/H_{A-F}(T) & \text{if } H < H_{A-F}, \\ 1 & \text{otherwise,} \end{cases} \quad (4)$$

where $H_{A-F}(T) = H_A(T) + 2H_E(T)$ is the characteristic field corresponding to the phase transition of twin from antiferromagnetic to ferromagnetic state, that is, to the state with $\theta(H, T) = 0$. In the theory of antiferromagnetism, this field is called a spin-flip field.

As it is known, the dynamic equations for magnetization vectors have a form

$$\begin{aligned} \frac{1}{\gamma} \cdot \frac{d\mathbf{M}_1}{dt} &= \frac{\partial F}{\partial \mathbf{M}_1} \times \mathbf{M}_1, \\ \frac{1}{\gamma} \cdot \frac{d\mathbf{M}_2}{dt} &= \frac{\partial F}{\partial \mathbf{M}_2} \times \mathbf{M}_2, \end{aligned} \quad (5)$$

where γ is gyromagnetic ratio. Following the standard procedure, the magnetization vectors are presented as the sums of equilibrium and variable parts,

$$\mathbf{M}_{1,2} = \bar{\mathbf{M}}_{1,2} + \mathbf{m}_{1,2}(t) \quad (6)$$

where $\mathbf{m}_{1,2}(t) \propto \exp(i\omega t)$, t is time, and ω is angular frequency. It is advantageous to transform the dynamic equations into the equation systems for the variables

$$\mathbf{l} = \mathbf{m}_1 - \mathbf{m}_2, \quad \mathbf{m} = \mathbf{m}_1 + \mathbf{m}_2, \quad (7)$$

which are the variable parts of the vector of ferromagnetism $\mathbf{M} = \mathbf{M}_1 + \mathbf{M}_2$ and vector of antiferromagnetism $\mathbf{L} = \mathbf{M}_1 - \mathbf{M}_2$, widely used in the theory of magnetism [32].

The linearized equation system for the components of vector \mathbf{l} is

$$\begin{aligned} i\omega l_x &= \gamma[H - (H_A + 2H_E \cos \theta)]l_y, \\ i\omega l_y &= -\gamma[H - (H_A + 2H_E \cos \theta)]l_x. \end{aligned} \quad (8)$$

The terms, which are proportional to $m_z \sim l_i^2 \ll l_i$, are omitted in the course of linearization of dynamic equations. The resonance frequency for vector \mathbf{l} oscillations is obtained by equating to zero the determinant of equation system [Eq. (8)]. This frequency is

$$\omega_l = \gamma[H - (H_A + 2H_E) \cos \theta] \quad (9)$$

Taking into account Eqs. (4) and (9), one can see that $\omega_l = 0$ if $H < H_{A-F}$ and

$$\omega_l = \gamma(H - H_A - 2H_E) \quad (10)$$

otherwise.

The linearized equation system for the components of vector \mathbf{m} is

$$\begin{aligned} i\omega m_x &= \gamma(H - H_A \cos \theta)m_y - H_A \sin \theta l_z, \\ i\omega m_y &= -\gamma(H - H_A \cos \theta)m_x, \\ i\omega l_z &= 2H_E \sin \theta m_x. \end{aligned} \quad (11)$$

The resonance frequency for vector \mathbf{m} oscillations is

$$\omega_m = \gamma[(H - H_A \cos \theta)^2 + 2H_A H_E \sin^2 \theta]^{1/2} \quad (12)$$

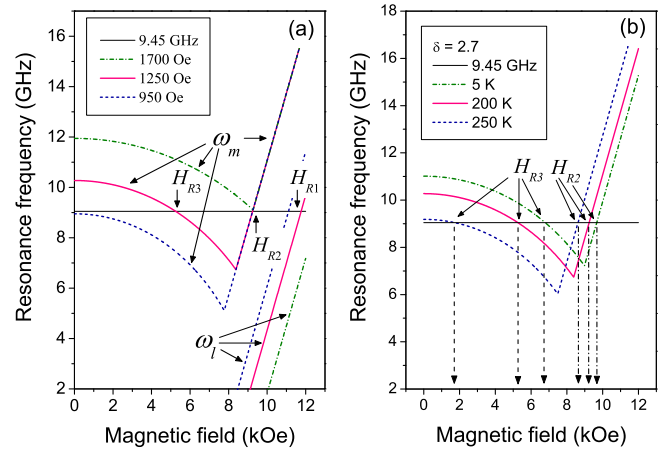


FIG. 7. Resonance frequencies computed from Eqs. (9) and (12) for the exchange fields of 950 Oe, 1250 Oe, and 1700 Oe (a); the resonance field values corresponding to the exchange field of 1250 Oe are marked by the arrows. Resonance frequency ω_m computed from Eq. (12) for the fixed value of exchange constant and three temperature values (b); the vertical dash-dotted and dashed arrows point to the resonance field values H_{R2} and H_{R3} , respectively.

In the field range $H > H_{A-F}$, this frequency is equal to the ferromagnetic resonance frequency

$$\omega_{fm} = \gamma(H - H_A) \quad (13)$$

because in this field range the equilibrium directions of magnetization vectors of twin components are parallel to each other and to the axis z ; therefore, the film is in ferromagnetic state.

Let us accept that $M(0) = 500$ G (evaluated from Fig. 2 and dimensions of film), $T_C = 360$ K, and $H_A = 4\pi M$ (i.e., the magnetic anisotropy field is considered to be equal to magnetostatic field of the film). In this case, Eq. (2) results in the value $H_A = 5850$ Oe for the temperature of 200 K. Figure 7(a) shows the magnetic resonance frequencies computed for this anisotropy field and different values of the exchange field, H_E . The horizontal line shows the experimental value of microwave frequency. For all H_E values, the plots of function $\omega_l(H)$ are the straight lines, which cross the horizontal line. The cross points correspond to the observable values of resonance field, denoted as H_{R1} . The function $\omega_m(H)$ is a *non-monotonic* function for small values of the exchange field. Its plot crosses the horizontal line at *two* values of resonance field H_{R2} and H_{R3} if the exchange field value is larger than 950 Oe but smaller than 1700 Oe, that is if $2.1 < \delta < 3.6$. In this case, *three* resonance field values, H_{R1} , H_{R2} and H_{R3} , are observable at the microwave frequency of 9.45 GHz. In the case that $H_E < 950$ Oe, only the resonance fields H_{R1} and H_{R2} can be detected. If $H_E \geq 1700$ Oe, only the resonance field value H_{R1} can be detected at given microwave frequency. It should be noted that the $\omega_m(H)$ function becomes monotonic at $H_E > 3$ kOe.

Figure 7(b) depicts the dependencies of the resonance frequencies on the external magnetic field. The frequencies are computed for different temperatures. The vertical arrows point to the resonance field values corresponding to different temperatures. It is seen that both H_{R2} and H_{R3} values are

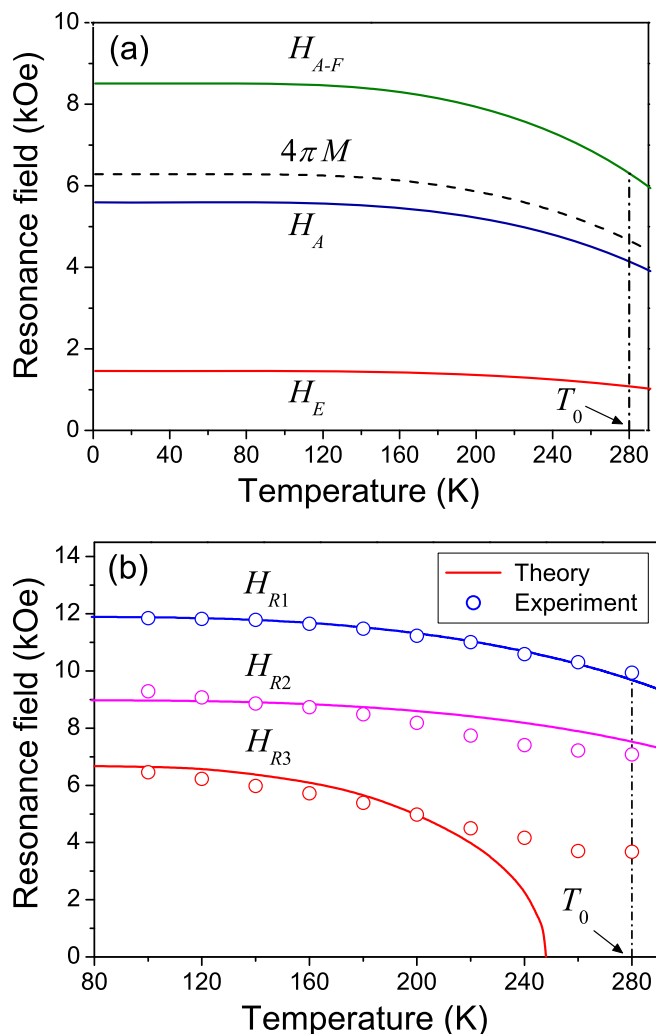


FIG. 8. Theoretical temperature dependencies of characteristic parameters of the martensitic $\text{Ni}_{46.0}\text{Mn}_{36.8}\text{Sn}_{11.4}\text{Co}_{5.8}/\text{MgO}(001)$ film (a); theoretical (lines) and experimental (circles) temperature dependencies of the resonance fields (b). The temperature T_0 approximately corresponds to the start of reverse MT.

the decreasing functions of temperature, but the temperature dependence of H_{R3} is more pronounced.

V. EXTRACTION OF THE COUPLING PARAMETERS FOR $\text{Ni}_{46.0}\text{Mn}_{36.8}\text{Sn}_{11.4}\text{Co}_{5.8}/\text{MgO}(001)$ FILM

Magnetic measurements performed for the $\text{Ni}_{46.0}\text{Mn}_{36.8}\text{Sn}_{11.4}\text{Co}_{5.8}/\text{MgO}(001)$ film show that the low-temperature limit of $M(T)$ function, $M(0)$, is approximately equal to 500 G and that the Curie temperature is close to 360 K. The determination of coupling parameters was carried out as follows.

First, a magnetic anisotropy constant, $\beta = 11.2$, and the magnetic anisotropy field, $H_A(T)$, were determined from Eq. (13) by fitting the theoretical curve $H_{R2}(T)$ to the experimental points in the temperature range from 100 K to 200 K [see Figs. 8(a) and 8(b)]. A good agreement between theoretical and experimental values of H_{R2} was observed in the whole temperature range of martensitic phase [Fig. 8(b)].

The value of parameter β is close to the magnetostatic value 4π [see Fig. 8(a)]. It points to the negligibly small uniaxial magnetocrystalline anisotropy of the twinned film.

Second, the spin exchange constant, $\delta = 2.92$, and the characteristic field, $H_E(T)$, were determined from Eq. (10) by fitting the theoretical $H_{R1}(T)$ curve to the experimental points. Figure 8(b) shows an excellent agreement between theoretical and experimental dependences $H_{R1}(T)$, achieved using the functions $H_A(T)$ and $H_E(T)$ presented in Fig. 8(a). This fact confirms the applicability of Eq. (2) for the $M(T)$ function to the studied film and the correctness of acceptance for computation T_C value.

Third, the theoretical dependence $H_{R3}(T)$ was determined from Eq. (12) without additional fitting of characteristic parameters of the film. A good agreement between theoretical and experimental data was observed in the temperature range from 100 K to 220 K [see Fig. 8(b)]. The disagreement between theory and experiment in the temperature range $220 \text{ K} < T < T_0$ can be caused by the weak dependence of ω_m on the magnetic field at low fields. Almost flat segments are present in the $\omega_m(H)$ curves for $H < 2 \text{ kOe}$ (Fig. 7). Considering the decrease of the microwave frequency by $\Delta\omega \sim 0.1 \text{ GHz}$ results in the increase of the resonance field from zero to 2 kOe. Moreover, the lattice instability in the MT temperature range may cause the temperature variation of the parameters β and δ . However, the experimental study of such variations is a complicated problem.

VI. SUMMARY AND CONCLUSION

We have carried out a ferromagnetic resonance and magnetization study of epitaxial $\text{Ni}_{46.0}\text{Mn}_{36.8}\text{Sn}_{11.4}\text{Co}_{5.8}/\text{MgO}(001)$ films exhibiting the MT at 270 K. The magnetic resonance measurements reveal one resonance line in the austenitic phase and three lines in the twinned martensitic phase. Magnetization measurements show that the ferromagnetic ordering dominates in both phases; therefore, only one resonance line should be observed. A quantitative theoretical analysis of the magnetic resonance spectrum was developed, enabling explanation of the appearance of three resonance lines in the martensitic phase, assuming a weak antiferromagnetic exchange interaction between the ferromagnetic twin components in the martensitic film.

The dimensionless magnetic anisotropy constant $\beta = 11.2$ and exchange constant $\delta = 2.92$ were evaluated by fitting the computed resonance fields $H_{R1}(T)$ and $H_{R2}(T)$ to experimental values. A quantitative agreement between the positions of computed and measured resonance lines was achieved. A good agreement between the theoretical and experimental values of the resonance field $H_{R3}(T)$ was observed without additional fitting of the material constants. The determined value of exchange constant corresponds to the very low exchange field, about 1.5 kOe, because the number of magnetic ions interacting antiferromagnetically through the twin boundary is much less than the total number of magnetic ions in the twin. A similar situation takes place in artificial antiferromagnetic structures such as those used in giant magnetoresistance devices and spin valves.

In conclusion, there exists a strong resemblance between the artificial antiferromagnetic superlattices and twinned

martensite in the studied films. In both physical systems, a weak antiferromagnetic coupling between the ferromagnetically ordered layers (in the superlattices) and twin components (in the twinned martensite) is present. Because of the possible applications, this resemblance deserves careful study [33]. It also implies an emerging vision of the so called nonmagnetic martensite in MMSMAs, which are under continuing development.

ACKNOWLEDGMENTS

Financial support from the Spanish Ministry of Economy and Competitiveness (MINECO) (Projects No. MAT2014-56116-C04-02 and No. MAT2014-56116-C04-03) and the Portuguese Foundation of Science and Technology (FCT) through the Project EXPL/IF/00981/2013 and “Investigador FCT” program is acknowledged.

-
- [1] *Heusler Alloys. Properties, Grows, Applications*, edited by C. Felser and A. Hirohata, Springer Series in Material Science (Springer-Verlag, Berlin, 2016), Vol. 222.
- [2] S. J. Murray, M. Marioni, S. M. Allen, R. C. O’Handley, and T. A. Lograsso, *Appl. Phys. Lett.* **77**, 886 (2000).
- [3] O. Heczko, A. Sozinov, and K. Ullakko, *IEEE Trans. Mag.* **36**, 3266 (2000).
- [4] M. Acet, L. Manosa, and A. Planes, in *Handbook of Magnetic Materials*, edited by K. H. J. Buschow (Elsevier, Amsterdam, 2011), Vol. 19, pp. 231–289.
- [5] A. Planes, L. Mañosa, and M. Acet, *J. Phys.: Condens. Matter* **21**, 233201 (2009).
- [6] *Disorder and Strain-Induced Complexity in Functional Materials*, edited by T. Kakeshita, T. Fukuda, A. Saxena, and A. Planes, Springer Series in Material Science (Springer, Berlin, 2012), Vol. 148.
- [7] Y. Sakuraba, M. Hattori, M. Oogane, Y. Ando, H. Kato, A. Sakuma, T. Miyazaki, and H. Kubota, *Appl. Phys. Lett.* **88**, 192508 (2006).
- [8] *Magnetic Nanostructures, Spin Dynamics and Spin Transport*, edited by H. Zabel and M. Farle (Springer-Verlag, Berlin, 2013).
- [9] R. Y. Umetsu, X. Xu, and R. Kainuma, *Scr. Mater.* **116**, 1 (2016).
- [10] V. N. Prudnikov, A. P. Kazakov, I. S. Titov, N. S. Perov, A. B. Granovskii, I. S. Dubenko, A. K. Pathak, N. Ali, A. P. Zhukov, and J. Gonzalez, *JETP Lett.* **92**, 666 (2010).
- [11] T. Krenke, E. Duman, M. Acet, E. F. Wassermann, X. Moya, L. Mañosa, and A. Planes, *Nat. Mater.* **4**, 450 (2005).
- [12] V. A. L’vov, A. Kosogor, J. M. Barandiaran, and V. A. Chernenko, *J. Appl. Phys.* **119**, 013902 (2016).
- [13] R. Kainuma, K. Ito, W. Ito, R.Y. Umetsu, T. Kanomata, and K. Ishida, *Mater. Sci. Forum* **635**, 23 (2010).
- [14] D. Y. Cong, S. Roth, J. Liu, Q. Luo, M. Pötschke, C. Hurrich, and L. Schultz, *Appl. Phys. Lett.* **96**, 112504 (2010).
- [15] D. Y. Cong, S. Roth, and L. Schultz, *Acta Mater.* **60**, 5335 (2012).
- [16] J. I. Perez-Landazabal, V. Recarte, V. Sanchez-Alarcos, C. Gomez-Polo, and E. Cesari, *Appl. Phys. Lett.* **102**, 101908 (2013).
- [17] V. D. Buchelnikov, V. V. Sokolovskiy, S. V. Taskaev, V. V. Khovaylo, A. A. Aliev, L. N. Khanov, A. B. Batdalov, P. Entel, H. Miki, and T. Takagi, *J. Phys. D: Appl. Phys.* **44**, 064012 (2011).
- [18] P. Entel, M. E. Gruner, D. Comtesse, and M. Wuttig, *JOM* **65**, 1540 (2013).
- [19] M. Acet and E. F. Wassermann, *Adv. Eng. Mater.* **14**, 523 (2012).
- [20] P. Lázpita, J. Escolar, V. A. Chernenko, and J. M. Barandiarán, *JALCOM* **644**, 883 (2015).
- [21] I. R. Aseguinolaza, V. Golub, J. M. Barandiarán, M. Ohtsuka, P. Müllner, O. Y. Salyuk, and V. A. Chernenko, *Appl. Phys. Lett.* **102**, 182401 (2013).
- [22] V. A. Chernenko, V. A. Lvov, V. Golub, I. R. Aseguinolaza, and J. M. Barandiarán, *Phys. Rev. B* **84**, 054450 (2011).
- [23] J. Nagues and I. K. Schuller, *J. Magn. Magn. Mater.* **192**, 203 (1999).
- [24] Q. L. Ma, X. M. Zhang, T. Miyazaki, and S. Mizukami, *Sci. Rep.* **5**, 7863 (2015).
- [25] V. V. Kruglyak, S. O. Demokritov, and D. Grundler, *J. Phys. D: Appl. Phys.* **43**, 264001 (2010).
- [26] V. A. Chernenko, V. Golub, J. M. Barandiaran, O. Y. Salyuk, F. Albertini, L. Righi, S. Fabbrici, and M. Ohtsuka, *Appl. Phys. Lett.* **96**, 042502 (2010).
- [27] P. Klaer, T. Eichhorn, G. Jakob, and H. J. Elmers, *Phys. Rev. B* **83**, 214419 (2011).
- [28] A. Auge, N. Teichert, M. Meinert, G. Reiss, A. Hutten, E. Yüzüak, I. Dincer, Y. Elerman, I. Ennen, and P. Schattschneider, *Phys. Rev. B* **85**, 214118 (2012).
- [29] Y. Luo, P. Leicht, A. Laptev, M. Fonin, U. Rüdiger, M. Laufenberg, and K. Samwer, *New J. Phys.* **13**, 013042 (2011).
- [30] S. Foner, in *Magnetism*, edited by G. T. Rado and H. Suhl (Academic Press, New York, London, 1963), Vol. 1.
- [31] Z. Zhang, L. Zhou, P. E. Wigen, and K. Ounadjela, *Phys. Rev. B* **50**, 6094 (1994).
- [32] S. V. Vonsovskii, *Magnetism* (Wiley, New York, 1974).
- [33] T. Devolder, *J. Appl. Phys.* **119**, 153905 (2016).